

Evolutionary and pulsational properties of low-mass white dwarf stars with oxygen cores resulting from close binary evolution

L. G. Althaus,^{1★†} A. H. Córscico,^{1★‡} A. Gautschy,² Z. Han,^{3★} A. M. Serenelli^{1★‡}
and J. A. Panei^{1★‡}

¹*Facultad de Ciencias Astronómicas y Geofísicas de la Universidad Nacional de La Plata and Instituto de Astrofísica de La Plata (CONICET-UNLP), Paseo del Bosque S/N, (1900) La Plata, Argentina*

²*Frobbergstr. 43, 4052 Basel, Switzerland*

³*National Astronomical Observatories/Yunnan Observatory, The Chinese Academy of Science, PO Box 110, Kunming 650011, China*

Accepted 2003 September 4. Received 2003 August 29; in original form 2003 May 30

ABSTRACT

The present work is designed to explore the evolutionary and pulsational properties of low-mass white dwarfs with carbon/oxygen cores. In particular, we follow the evolution of a $0.33\text{-}M_{\odot}$ white dwarf remnant in a self-consistent way with the predictions of nuclear burning, element diffusion and the history of the white dwarf progenitor. Attention is focused on the occurrence of hydrogen shell flashes induced by diffusion processes during cooling phases. The evolutionary stages prior to the white dwarf formation are also fully accounted for by computing the conservative binary evolution of an initially $2.5\text{-}M_{\odot}$ Population I star with a $1.25\text{-}M_{\odot}$ companion, and with period $P_i = 3\text{d}$. Evolution is followed down to the domain of the ZZ Ceti stars on the white dwarf cooling branch.

We find that chemical diffusion induces the occurrence of an additional hydrogen thermonuclear flash, which leads to stellar models with thin hydrogen envelopes. As a result, a fast cooling is encountered at advanced stages of evolution. In addition, we explore the adiabatic pulsational properties of the resulting white dwarf models. As compared with their helium-core counterparts, low-mass oxygen-core white dwarfs are characterized by a pulsational spectrum much more featured, an aspect which could eventually be used for distinguishing both types of stars, if low-mass white dwarfs were in fact found to pulsate as ZZ Ceti-type variables. Finally, we perform a non-adiabatic pulsational analysis on the resulting carbon/oxygen low-mass white dwarf models.

Key words: binaries: general – stars: evolution – stars: interiors – stars: oscillations – white dwarfs.

1 INTRODUCTION

Low-mass white dwarf (WD) stars, having masses less than $\approx 0.5 M_{\odot}$, are the result of evolution of certain close binary systems (Paczynski 1976a; Iben & Webbink 1989; Iben & Livio 1993). Indeed, mass-transfer episodes in binary systems are required to form low-mass WDs. An isolated star of comparable low mass would take more than a Hubble time to evolve into a corresponding WD configuration. The low-mass WDs are thought to have a core composed

by helium; their binary nature was first put on a firm observational basis by Marsh (1995) and Marsh, Dhillon & Duck (1995). Since then, low-mass WDs have been detected in numerous binary configurations containing usually either another WD or a neutron star (see, e.g. Lundgren et al. 1996; Moran, Marsh & Bragaglia 1997; Orosz et al. 1999; Maxted et al. 2000; van Kerkwijk et al. 2000). In addition, several low-mass WDs have been found in open and globular clusters (Landsman et al. 1997; Edmonds et al. 1999, 2001; Taylor et al. 2001). Evolutionary models for helium-core WDs have been calculated by Hansen & Phinney (1998), Driebe et al. (1998); Sarna, Ergma & Antipova (2000), Althaus, Serenelli & Benvenuto (2001a,b) and Serenelli et al. (2002).

However, theoretical evidence casts some doubt on all low-mass WDs indeed being helium-core WDs. In fact, Iben & Tutukov (1985) proposed several scenarios where low-mass WDs could harbour cores with elements heavier than helium. More recently, Han, Tout & Eggleton (2000) have carried out new close binary evolutionary

*E-mail: althaus@fcaglp.unlp.edu.ar (LGA); acorsico@fcaglp.unlp.edu.ar (AHC); zhanwen@public.km.yn.cn (ZH); aldost@MPA-Garching.MPG.DE (AMS); panei@fcaglp.unlp.edu.ar (JAP)

†Member of the Carrera del Investigador Científico y Tecnológico, CONICET, Argentina.

‡Fellow of CONICET Argentina.

calculations and found that some of the presumed helium-core WDs in double degenerate systems may actually be WDs with carbon/oxygen cores. Specifically, their calculations show that, if the onset of mass transfer episodes takes place after the end of central hydrogen burning during the middle Hertzsprung-gap stage, a carbon/oxygen WD with mass as low as $0.33 M_{\odot}$ may be formed from stable Roche lobe overflow (RLOF) if the initial mass of the primary star is close to $2.5 M_{\odot}$.

The present work aims at exploring the evolution of low-mass WDs with carbon/oxygen cores in a self-consistent way with the predictions of nuclear burning, time-dependent element diffusion and the history of the WD progenitor. We concentrate on a carbon/oxygen-core WD remnant of mass $0.33 M_{\odot}$. Attention is focused on the occurrence of hydrogen shell flashes and the role played by diffusion processes during cooling phases. The evolutionary stages prior to the WD formation are also fully accounted for by computing the conservative binary evolution of an initially $2.5 - M_{\odot}$ Population I star with a $1.25 - M_{\odot}$ companion, and with period $P_i = 3d$. Finally, we explore the adiabatic and non-adiabatic pulsational properties of the resulting WD models and we compare them with those of helium-core WDs.

In this work, we hope to address essentially the two following questions: (i) what is the role of element diffusion in the evolution of low-mass, carbon/oxygen WDs?; and (ii) what differences in the evolutionary properties as well as in the pulsational signal (if these objects do actually pulsate) can we expect between low-mass WDs with helium cores and those with carbon/oxygen cores? In Section 2, we describe the main physical inputs of the models. In Section 3, we present the evolutionary results, particularly regarding the WD stages. Section 4 contains the discussion of the pulsational properties of our models. Finally, Section 5 is devoted to summarizing our results and making some concluding remarks.

2 INPUT PHYSICS AND COMPUTATIONAL DETAILS

The evolutionary code used in this work to simulate the binary evolution is that described by Han et al. (2000) and references therein. The code uses a self-adaptive non-Lagrangian mesh and is based on an up-to-date physical description such as Opacity Library (OPAL) radiative (Rogers & Iglesias 1992) and molecular (Alexander & Ferguson 1994) opacities, a detailed equation of state that includes coulomb interactions and pressure ionization and nuclear reaction rates from Caughlan et al. (1985) and Caughlan & Fowler (1988). Convective overshooting is not considered.

For the WD regime, we employed the LPCODE evolutionary code which has been used in previous works on WD evolution. The code has been developed at La Plata Observatory and it is described in Althaus (1996), Althaus et al. (2001a), Serenelli (2002), Althaus et al. (2003) and references therein. As for the constitutive physics, LPCODE employs OPAL radiative opacities (including carbon- and oxygen-rich compositions) for arbitrary metallicity from Iglesias & Rogers (1996). Opacities for various metallicities are required during the WD cooling regime in view of the metallicity gradients that develop as a result of gravitational settling (see below). The equation of state is an updated version of that of Magni & Mazzitelli (1979). High-density conductive opacities and the various mechanisms of neutrinos emission are taken from the works of Itoh and collaborators (see Althaus 1996). Hydrogen burning is taken into account by considering a complete network of thermonuclear reaction rates corresponding to the proton-proton chain and the CNO bi-cycle. Nuclear reaction rates are taken from Caughlan &

Fowler (1988). Electron screening is treated as in Wallace, Woosley & Weaver (1982).

An important aspect of the present study is the evolution of the chemical abundance distribution caused by element diffusion during the whole WD stage. In our treatment of time-dependent diffusion, we have considered the following nuclear species: ^1H , ^3He , ^4He , ^{12}C , ^{14}N and ^{16}O . The chemical evolution resulting from element diffusion is described in LPCODE, for a given isotope i having a number density n_i , by the continuity equation as

$$\frac{\partial n_i}{\partial t} = -\frac{1}{r^2} \frac{\partial}{\partial r} (r^2 n_i w_i), \quad (1)$$

where w_i is the diffusion velocity as given by the solution of the multicomponent flow equations describing gravitational settling, chemical and thermal diffusion (Burgers 1969). Because we are interested in the chemical evolution occurring quite deep in the star, radiative levitation (which is expected to modify the surface composition of hot WDs) has been neglected. In terms of the gradient of ion densities, diffusion velocities can be written in the form

$$w_i = w_i^{\text{st}} - \sum_{\text{ions}(j)} \sigma_{ij} \frac{d \ln n_j}{dr}, \quad (2)$$

where w_i^{st} stands for the velocity component due to gravitational settling and thermal diffusion and σ_{ij} represent the components due to the gradients in number density (chemical diffusion). Details are given in Althaus et al. (2001a) and Gautschy & Althaus (2002). We want to mention that after computing the change of abundances by effect of diffusion, they are evolved according to nuclear reactions and convective mixing. It is worth mentioning that radiative opacities are calculated for metallicities consistent with diffusion predictions. In particular, the metallicity is taken as twice the abundances of CNO elements.

In this work, we have followed the *complete* evolution of an initially $2.5 - M_{\odot}$ star in a close binary system from the main sequence through the mass transfer episodes to the domain of the ZZ Ceti stars on the WD cooling branch. Specifically, the initial mass of the primary and secondary stars is 2.5 and $1.25 M_{\odot}$, respectively, with an initial orbital period of $P_i = 3d$. A solar-like initial composition $(Y, Z) = (0.28, 0.02)$ was adopted. The treatment of convection is that of the mixing-length theory, with the ratio of the mixing length to the local pressure scaleheight set to 2 (see Han et al. 2000 for details). The onset of RLOF, which is assumed to be conservative, occurs after the central hydrogen exhaustion in the middle of the Hertzsprung-gap stage. After mass transfer episodes, the mass of the WD remnant is $0.33 M_{\odot}$. As stated in the introduction, one of the aims of this investigation is the exploration of the influence that diffusion has on the evolution of low-mass, carbon/oxygen WDs. Thus, in addition to evolutionary models in which diffusion is considered, we have computed the WD evolution for the case when diffusion is neglected. This allowed us to identify clearly the effect induced by diffusion on the evolution of such objects.

3 EVOLUTIONARY RESULTS

In the following, we describe the evolution on the Hertzsprung-Russell diagram (HRD) of the WD progenitor. Specifically, in Fig. 1, we show the HRD of the primary star, which initially has a stellar mass of $2.5 M_{\odot}$. The primary evolves from zero-age main sequence (point A) and burns hydrogen at its centre. After central hydrogen is exhausted, the star evolves to the Hertzsprung gap and fills its Roche lobe at point B, and the RLOF phase begins. The envelope mass is transferred to the secondary, which initially has a stellar

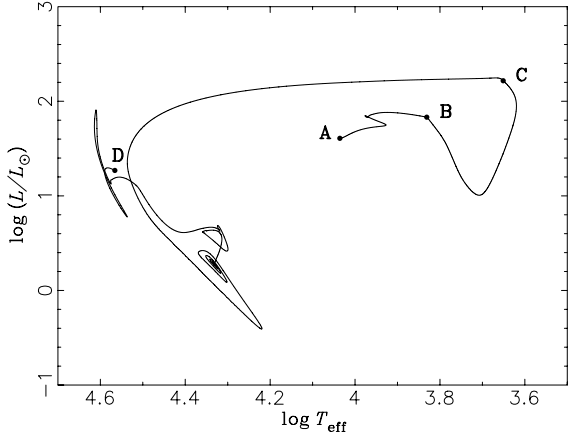


Figure 1. Hertzsprung–Russell diagram for the primary star during the binary evolution stage and core helium burning stages. Labels along the track denote specific stages during the evolution and are discussed in the text.

mass of $1.25 M_{\odot}$, until RLOF finally stops at point C. After RLOF, the primary becomes a helium star (with a thin hydrogen layer). As a result of mass loss episodes, the stellar mass has decreased to $M_{1f} = 0.3293 M_{\odot}$, whereas the mass of the secondary is now $M_{2f} = 3.4207 M_{\odot}$ and the orbital period has increased to $P_f = 64.08$ d. The helium star contracts and moves quickly across the HRD. Helium is ignited at the centre and the star experiences ‘breathing pulses’ (the loops at lower-left corner of the figure; see e.g. Castellani et al. 1985; Han et al. 2002). After central helium-burning, the star has an almost pure oxygen core of $0.11 M_{\odot}$. The evolution calculation of the resulting oxygen-core WD is continued from point D.

The resulting WD binary system continues to evolve; the secondary will fill its Roche lobe as an asymptotic giant branch (AGB) star and leads to the onset of another RLOF. The star has a CO core and a deep convective envelope. The mass transfer is dynamically unstable and a common envelope (CE; Paczyński 1976a) is formed. The CE engulfs the CO core and the primary (a WD). A large amount of orbital energy is deposited into the CE due to the friction between the CE and the embedded binary. The CE may be ejected if the orbital energy released can overcome the binding energy of the envelope, and leads to the formation of a binary system with two WD components, i.e. a double degenerate. If the common envelope ejection efficiency is $\alpha_{CE} = 1$ and thermal contribution to CE ejection is $\alpha_{th} = 1$ (see Han 1998; Han et al. 2002 for the definitions), the double degenerate system will have $M_1 = 0.3293 M_{\odot}$, $M_2 = 0.6572 M_{\odot}$, $P = 0.1837$ d. However, if $\alpha_{CE} = \alpha_{th} = 0.75$, the orbital period of the double degenerate will be 0.0735 d instead.

In the following, we describe the main evolutionary results for the WD evolution of the $0.33 - M_{\odot}$ oxygen-core remnant. In Figs 2 and 3, we show the HRDs for the WD remnant when element diffusion is neglected and when diffusion is considered, respectively. Labels along the track from A to H represent evolutionary stages for models with diffusion, the main characteristics of which are listed in Table 1. In both cases, evolution is characterized by the occurrence of several episodes of thermonuclear flashes during which the star experiences extensive loops in the HRD. Each of these loops results from unstable nuclear burning at the bottom of the hydrogen-rich envelope. Note that when diffusion is considered, the model experiences an additional thermonuclear flash, as compared with the situation of no diffusion. This last flash is triggered by chemical diffusion which,

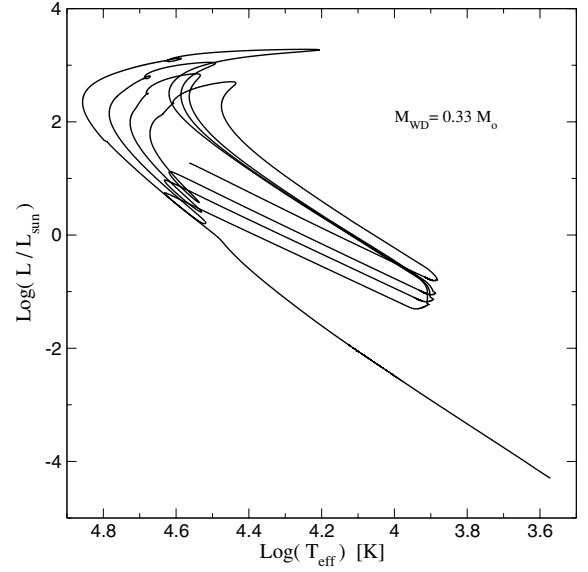


Figure 2. Hertzsprung–Russell diagram for the WD evolution of the $0.33 - M_{\odot}$ oxygen-core remnant when element diffusion is neglected. The WD experiences four hydrogen-shell flash episodes before reaching the final cooling branch.

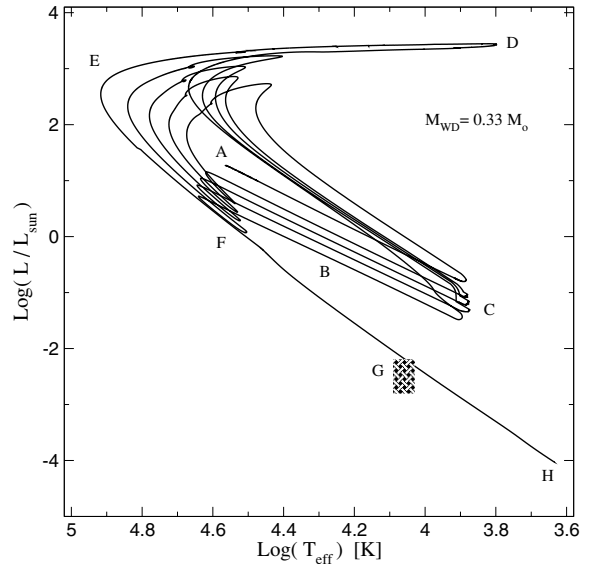


Figure 3. The same as Fig. 2, but for the case when element diffusion is considered. Letters at various positions along the track indicate selected stages of the evolution described in Table 1. Also, the approximate location of the domain of the ZZ Ceti instability strip is shown as a small shaded region. As a result of hydrogen chemically diffusing inwards during the cooling track, the WD experiences an additional thermonuclear flash, as compared with the situation of no diffusion. As a result of this diffusion-induced flash, the star is forced to evolve back to the red giant domain for a brief time interval (point D).

as the WD evolves along the cooling branch, carries some hydrogen inwards to hotter layers, where it burns unstably.¹ As we shall see,

¹ The occurrence of diffusion-induced hydrogen shell flashes is a theoretically known phenomena found in some detailed WD evolutionary calculations (see, for instance, Iben & MacDonald 1986 in the context of intermediate-mass, carbon/oxygen WDs).

Table 1. Selected stages for $0.33 - M_{\odot}$ oxygen-core WD models considering element diffusion, as labelled in Fig. 3. From left to right, the columns detail surface luminosity, effective temperature, age, surface gravity, nuclear luminosity, surface hydrogen abundance and hydrogen envelope mass.

| | $\text{Log}(L/L_{\odot})$ | $\text{Log}(T_{\text{eff}})$ | Age (10^6 yr) | $\text{Log}(g)$ | $\text{Log}(L_{\text{nuc}}/L_{\odot})$ | X_H | $\text{Log}(M_H/M_{\odot})$ |
|-----|---------------------------|------------------------------|------------------|-----------------|--|-------|-----------------------------|
| (A) | 1.2715 | 4.5640 | 0.000 | 5.8952 | 2.843 | 0.573 | -2.9003 |
| (B) | -0.4906 | 4.2337 | 7.797007 | 6.3360 | 5.218 | 1.000 | -3.4008 |
| (C) | -1.4003 | 3.8962 | 7.797009 | 5.8957 | 4.657 | 1.000 | -3.4008 |
| (D) | 3.4317 | 3.7982 | 7.797042 | 0.6717 | 3.2980 | 0.304 | -3.4008 |
| (E) | 2.5554 | 4.9168 | 7.81 | 6.0225 | 2.544 | 0.476 | -3.5674 |
| (F) | 0.0000 | 4.5066 | 7.98 | 6.9369 | -1.499 | 1.000 | -3.5987 |
| (G) | -1.9967 | 4.100 | 184.2 | 7.3095 | -2.968 | 1.000 | -3.6502 |
| (H) | -4.0289 | 3.635 | 4085 | 7.4791 | -6.982 | 1.000 | -3.6567 |

Ages are counted from point A, which corresponds to an evolutionary stage just before the onset of the first thermonuclear flash. The surface hydrogen abundance is evaluated at a mass depth of $10^{-10}M_*$ below the stellar surface.

the occurrence of this diffusion-induced thermonuclear flash is critical regarding the subsequent evolution of the remnant even during its final cooling phase. It is worth noting that the diffusion-induced flash is the most energetic one; as a result, the star – for a brief time interval – reaches giant dimensions again (point D). After this flash episode, the remnant eventually settles on its terminal cooling track.

The time dependence of the surface hydrogen abundance and the mass of the hydrogen envelope for the evolutionary stages following the end of the pre-WD evolution is illustrated in Fig. 4. The role of element diffusion is clearly emphasized by this figure. During each short-lived flash episode, convection reaches deep enough into

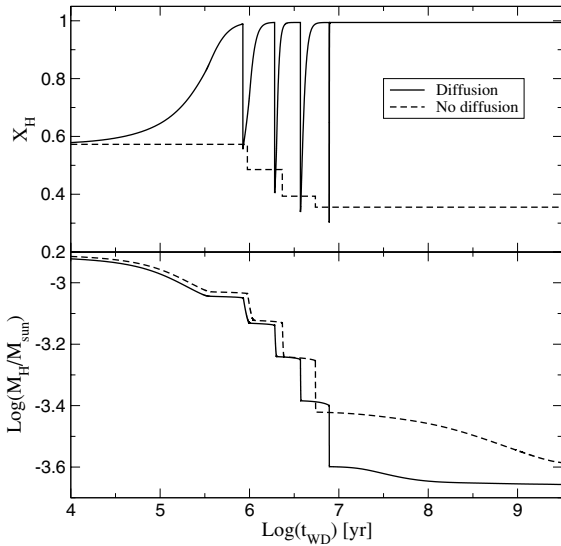


Figure 4. Abundance by mass of hydrogen at a mass depth of $10^{-10}M_*$ below the stellar surface (upper panel) and mass of the hydrogen envelope in solar units (lower panel) as a function of WD age for the $0.33 - M_{\odot}$ oxygen WD model. Solid lines correspond to the case when element diffusion is considered and dashed lines correspond to the case when diffusion is neglected. At each flash episode, the surface abundance of hydrogen is abruptly reduced as a result of convective mixing. Afterwards, diffusion causes the bulk of hydrogen to float on the surface again. Note also that during each flash episode, the mass of the hydrogen envelope is considerably reduced. Models with diffusion enter the final cooling branch (ages larger than 10^7 yr) with a markedly smaller hydrogen mass. By contrast, models without diffusion retain a larger hydrogen envelope which is burnt largely during the ensuing evolutionary stages.

the star to dredge helium up, thus leading to envelopes made up by hydrogen and helium. This is responsible for the steep declines of the surface hydrogen abundance. For models with diffusion, after each flash, the purity of the outer layers is rapidly re-established as soon as the star returns to the cooling branch. Note that the time intervals during which the envelope remains helium-enriched are indeed extremely short. This is in contrast to the predictions of models without diffusion. For these diffusion-free models, there is no physical process other than convection that can transport hydrogen to the surface. Thus, the final hydrogen abundance ($X_H \approx 0.35$) is established by the mixing episode that occurred during the last flash. The mass of the hydrogen envelope is shown in the lower panel of Fig. 4. An important feature revealed by this figure is that the remaining amount of hydrogen, shortly after hydrogen flashes have ceased, is markedly lower when diffusion is considered. Specifically, the hydrogen mass at the beginning of the final cooling track amounts to $M_H = 2.52 \times 10^{-4} M_{\odot}$, as compared with the $M_H = 3.82 \times 10^{-4} M_{\odot}$ that remains for the case when diffusion is neglected. The smaller hydrogen masses left in models with diffusion can be understood on the basis that, as the WD evolves along the cooling branch, the tail of the hydrogen distribution chemically diffuses inwards where the temperature is high enough to burn it – a process which, as we mentioned, eventually induces the occurrence of an additional thermonuclear flash. As can be seen, during this last flash episode, the total amount of hydrogen in the star is noticeably reduced as a result of the nuclear burning. As we shall see below, this fact produces a different cooling history even at very late stages of evolution.

It is important to note that when diffusion is neglected, an appreciable amount of hydrogen is processed *over the final cooling phase*. Accordingly, we expect that the role played by stable hydrogen shell burning during the final WD cooling phase is different according to whether element diffusion is considered or not – an expectation that is indeed borne out by the results shown in Fig. 5. In the upper panel of this figure, we depict the ratio of nuclear-to-surface luminosities as a function of WD age for the $0.33 - M_{\odot}$ oxygen-core WD. The solid line corresponds to the case when diffusion is included and the dashed line corresponds to the situation without diffusion. Only the evolutionary stages corresponding to the final cooling branch are depicted in the figure. Note that for these evolutionary stages of star models with diffusion, nuclear energy release never constitutes the main contribution to the radiated luminosity. In particular, as the WD evolves across the domain of the ZZ Ceti stars, nuclear burning contributes at most 10 per cent to the surface luminosity. It is worth mentioning that the nuclear

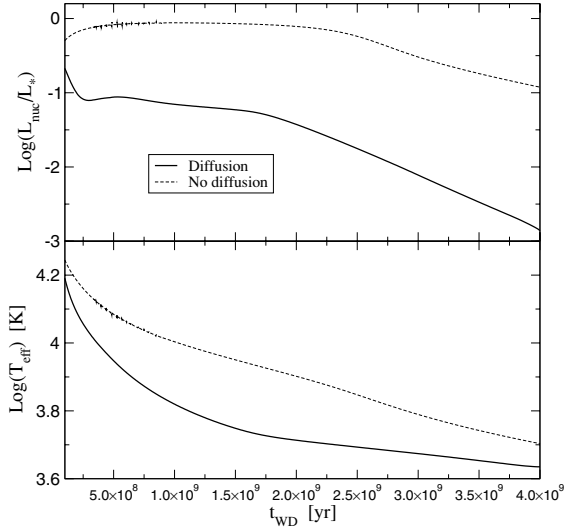


Figure 5. Ratio of nuclear-to-surface luminosities (upper panel) and effective temperature (lower panel) as a function of WD age for the $0.33 - M_{\odot}$ oxygen WD model. Solid lines correspond to the case when diffusion is considered and dashed lines correspond to the case when diffusion is neglected. Because the larger hydrogen envelope mass characterizes models without diffusion (see Fig. 4), hydrogen burning for such models is the dominant source of energy even at advanced stages of evolution, with the result that evolution is considerably slowed down.

energy production for effective temperatures lower than $\approx 11\,000$ K is almost entirely from the proton–proton chain. In fact, hydrogen burning via CNO-cycle reactions abruptly ceases by the time the WD has approached the hot edge of the ZZ Ceti instability strip. Eventually, hydrogen burning becomes virtually extinct at the lowest luminosities that we computed. These results are in contrast to the situation in which element diffusion is neglected. Here, stable hydrogen burning via proton-proton chain becomes the dominant energy source even at advanced stages of evolution. Note that for this situation, hydrogen burning contributes almost 80–90 per cent to surface luminosity, even at $T_{\text{eff}} \approx 8000$ K. Thus, we conclude that *element diffusion prevents hydrogen burning from being a main energy source for most of the evolution of a low-mass, oxygen-core WD*. This conclusion agrees with the predictions of Althaus et al. (2001a,b) for the case of low-mass, helium-core WDs.

Not surprisingly, the results mentioned above have strong implications regarding the evolutionary ages of the models. This is documented in the lower panel of Fig. 5, which illustrates the effective temperature versus the age of the WD. Again, the solid line corresponds to the evolutionary sequence with element diffusion. Note that when diffusion processes are considered, cooling ages become roughly a factor of 2–3 smaller. In fact, because nuclear reactions in models with diffusion do not dominate the energetics once the star has settled upon its final cooling track, to maintain its luminosity, the WD must extract energy from its relic thermal content, thus causing a much faster cooling. On the contrary, in the case of models without diffusion, evolution is dictated by residual hydrogen burning, giving rise to very long cooling ages. For instance, to reach $T_{\text{eff}} = 10000$ K, models with diffusion require 0.36 Gyr, whereas models without diffusion need about 1 Gyr.

We compare now the evolutionary properties of our $0.33 - M_{\odot}$ oxygen-core WD models with those of their helium-core counterparts. Specifically, the comparison is made with a $0.327 - M_{\odot}$ helium WD sequence with diffusion as calculated by Althaus et al.

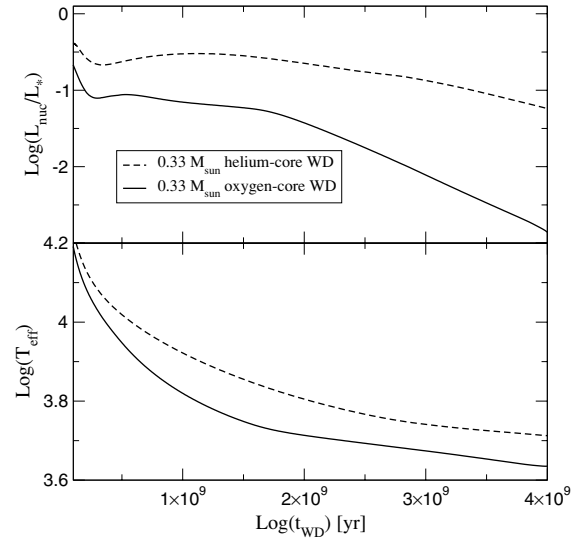


Figure 6. Ratio of nuclear-to-surface luminosities (upper panel) and effective temperature (lower panel) as a function of WD age for $0.33 - M_{\odot}$ WD sequences with diffusion. Solid and dashed lines correspond to the cases of oxygen-core and helium-core models, respectively. For both cases, hydrogen burning does not represent the main source of energy. Note that oxygen-core WDs evolve much more rapidly than their helium-core counterparts.

(2001a). We begin by examining the upper panel of Fig. 6, which illustrates the role of hydrogen burning as an energy source for both sequences during the final cooling phase. For the stages depicted in the figure, nuclear burning is not the dominant source of the luminosity of the star for both core compositions (see Althaus et al. 2001a for the evolutionary properties of helium-core WDs when diffusion is considered); thus, evolution is basically governed by the decrease of the thermal heat content of the star. As is well known, for a given mass, an oxygen core has a lower total capacity of storing heat than a helium core (we remind the reader that the specific heat is proportional to the number of particles; hence, per gram of material, the specific heat is inversely proportional to the atomic weight of the constitutive elements). Accordingly, we expect oxygen-core WDs to cool faster than helium-core ones. This expectation is confirmed by the lower panel of Fig. 6, which shows the time taken by objects to cool down to a given effective temperature. We find that, at advanced stages, to reach a given temperature, the oxygen-core WD has to evolve in about half the time a helium-core WD needs.

The shape of the chemical composition profile is critical regarding the pulsational properties of WDs. In particular, it contributes to the shape of the Ledoux term appearing in the Brunt-Väisälä frequency (Brassard et al. 1991) and plays a critical role in the phenomenon of mode trapping in WDs (see Brassard et al. 1992 and also Córscico et al. 2001). In Fig. 7, we show the abundance by mass of ^1H , ^4He , ^{12}C and ^{16}O as a function of the outer mass fraction for the $0.33 - M_{\odot}$ oxygen-core WD remnant. The upper panel depicts the abundance distribution shortly after the formation of the oxygen core and before the remnant experiences its first thermonuclear flash. The internal chemical profile emerging from the pre-WD evolution is characterized by an almost pure oxygen core of $0.08 M_{\odot}$. The oxygen core is surrounded by a shell rich in helium, carbon and oxygen with an overlying essentially pure helium buffer. The abundance distribution in the innermost regions is clearly different from that expected in the case of helium-core WDs, a feature which is expected to bear its signature in the theoretical period spectrum

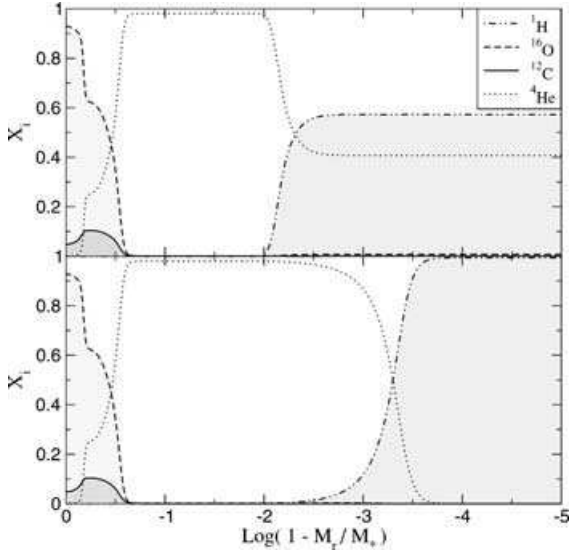


Figure 7. Chemical abundance distribution in terms of the outer mass fraction for the $0.33 - M_{\odot}$ oxygen-core WD. The upper panel corresponds to an evolutionary stage shortly after the formation of the oxygen core; the lower panel corresponds to an evolutionary stage near the ZZ Ceti instability strip. Note that element diffusion modifies the shape of the hydrogen and helium profiles markedly.

of these stars. The outermost layers are composed of helium and hydrogen. The abundance of these elements is different from those assumed for the interstellar medium because mass loss during the close binary evolution exposed layers in which hydrogen burning has occurred at earlier times. On the cooling track, the abundance distribution is altered by gravitational settling and chemical diffusion.² This is visualized in the lower panel of Fig. 7, which illustrates the resulting chemical profile when the WD has reached the domain of the ZZ Ceti instability strip on the final cooling branch. Note that element diffusion appreciably modifies the abundance distribution, particularly in the outer layers. Indeed, the hydrogen and helium profiles are markedly smoothed out by the time the ZZ Ceti domain is reached. At deeper layers, the diffusion time-scale becomes much longer than the evolutionary time-scale and the chemical profile remains thus fixed during the entire WD evolution.

The effect of diffusion on the element distribution within the star is emphasized in Fig. 8, where the abundances of ^1H , ^4He , ^{12}C , ^{14}N and ^{16}O are shown as a function of the outer mass fraction for $0.33 - M_{\odot}$ oxygen-core WD models at four selected epochs. The effect of diffusion on the element distribution is clearly noticeable. In particular, chemical diffusion moves a hydrogen tail inwards into hotter layers, causing the hydrogen burning rate to increase. At high T_{eff} values (panel b) this effect is responsible for the occurrence of the last flash episode. It is interesting to note that by the time the ZZ Ceti instability strip is reached (panel c), there exists an appreciable tail of hydrogen in the helium buffer. In fact, by this time, the hydrogen distribution reaches its maximum depth. At the same time, there are no metals in the outermost $2 \times 10^{-4} M_{\odot}$ of the star due to the occurrence of gravitational settling.

² It should be kept in mind that an appreciable fraction of the hydrogen envelope is consumed by nuclear burning during the flash episodes.

4 PULSATONAL ANALYSIS

We have seen that the evolutionary properties of the oxygen-core WDs differ appreciably from those of helium-core WDs, a fact which could eventually be used to shed light on the internal composition of observed low-mass WDs. However, a more promising and potential way of distinguishing both types of stars would be by means of the study of their pulsational patterns if low-mass WDs were in fact found to pulsate as ZZ-Ceti type variables. Although signs of variability in low-mass WDs have not been detected so far, we judge that an exploration of their oscillatory properties is nevertheless worthwhile. Indeed, in the context of more massive WDs, it is well known that asteroseismology is a very powerful tool for probing into the internal composition of degenerate stars (see, e.g. Bradley 1998; Metcalfe 2003). In particular, we are interested here in studying both the adiabatic and non-adiabatic pulsational properties.

4.1 Adiabatic pulsations

In order to explore the adiabatic pulsational properties of the WD models presented in this work, we have employed a general Newton–Raphson pulsational code coupled to the LPCODE evolutionary code, as detailed in Córscico et al. (2001, 2002; see also Córscico 2003). In particular, the computation of the Brunt–Väisälä frequency (N), an issue of fundamental relevance in the context of pulsating WD, is performed by adopting the prescription suggested by Brassard et al. (1991). Specifically, our code computes the so called ‘Ledoux term’ (B), given by

$$B = -\frac{1}{\chi_{\text{T}}} \sum_{i=1}^{n-1} \chi_{X_i} \frac{d \ln X_i}{d \ln P}, \quad (3)$$

with

$$\chi_{X_i} = \left(\frac{\partial \ln P}{\partial \ln X_i} \right)_{\rho, T, \{X_{j \neq i}\}} \quad (4)$$

and

$$\chi_{\text{T}} = \left(\frac{\partial \ln P}{\partial \ln T} \right)_{\rho, \{X_i\}}, \quad (5)$$

where X_i is the mass fraction of species i and ρ is the density.

Any local feature in the profiles of the internal chemical abundances is reflected by the Brunt–Väisälä frequency through the Ledoux term, as can be clearly noted from the following expression for N (Brassard et al. 1991):

$$N^2 = \frac{g^2 \rho}{P} \frac{\chi_{\text{T}}}{\chi_{\rho}} (\nabla_{\text{ad}} - \nabla + B). \quad (6)$$

Here, n is the number of ionic species present in the plasma, g is the local gravity, ∇_{ad} and ∇ are the adiabatic and actual temperature gradients, respectively, and

$$\chi_{\rho} = \left(\frac{\partial \ln P}{\partial \ln \rho} \right)_{T, \{X_i\}}. \quad (7)$$

In this section, we explore the adiabatic pulsational properties of low-mass, oxygen-core WD models and we compare them with those corresponding to the helium-core counterparts. Specifically, we have computed the adiabatic pulsational pattern of gravity modes corresponding to an evolutionary sequence of $0.33 - M_{\odot}$ oxygen-core WD models for an effective temperature range of 15 000–8000 K. Additionally, we have carried out pulsational calculations

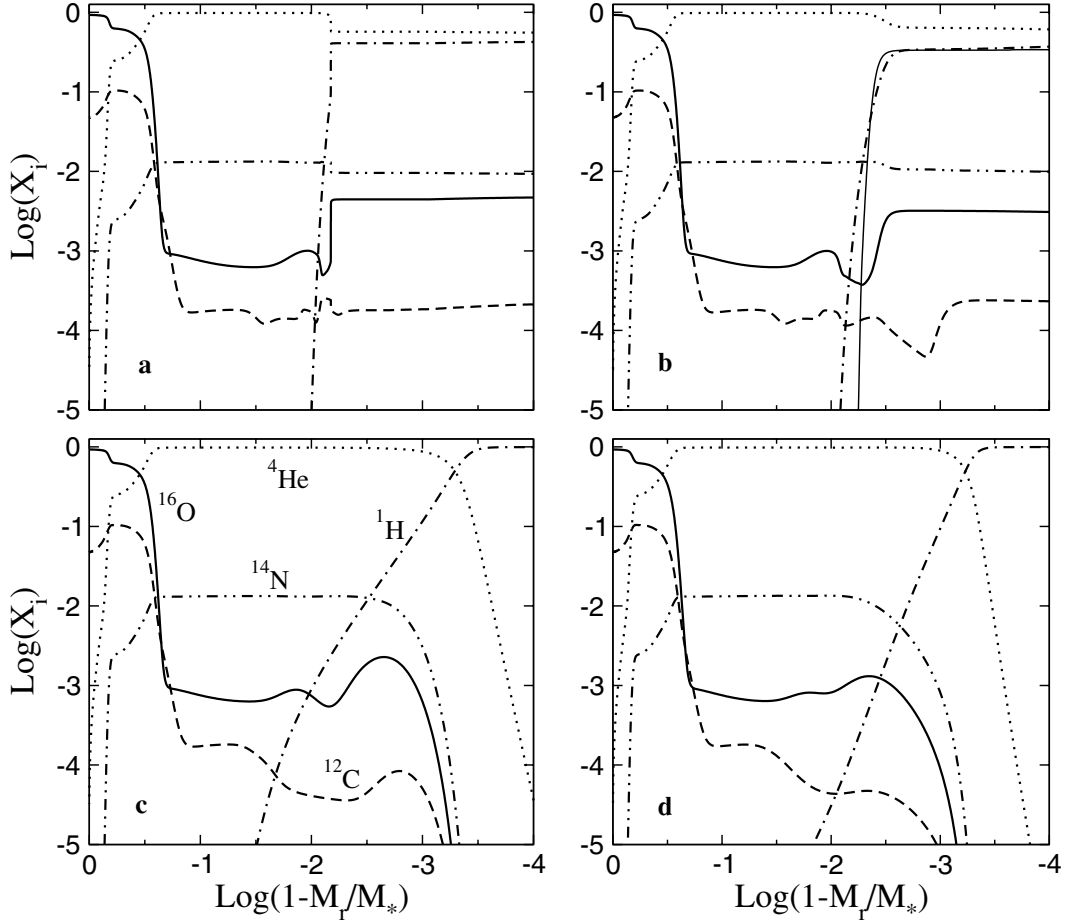


Figure 8. Chemical abundance distribution for ^1H , ^4He , ^{12}C , ^{14}N and ^{16}O as a function of the outer mass fraction for the $0.33 - M_{\odot}$ oxygen-core WD at four selected evolutionary stages. Panel a shows the chemical stratification during the second flash episode, shortly after the occurrence of the outer convective mixing. Panel b corresponds to the stage just before the occurrence of the last flash. To emphasize the importance of chemical diffusion, we also show with a thin solid line the hydrogen profile emerging from the previous flash. Panels c and d correspond to models on the final cooling branch: the ZZ Ceti domain and the last computed model, respectively. Note the role of both gravitational settling and chemical diffusion. In particular, chemical diffusion causes some hydrogen to reach deeper layers. At high T_{eff} values (panel b), this effect is responsible for the occurrence of the last flash episode. Values of $\log(L/L_{\odot})$ and $\log T_{\text{eff}}$ for panels a, b, c and d are, respectively: (0.96; 4.34), (0.72; 4.64), (-2.53; 3.98) and (-4.03; 3.63).

corresponding to an evolutionary sequence of $0.33 - M_{\odot}$ helium-core WD models for the same T_{eff} interval. To assess the mode-trapping/confinement features associated with both kind of objects, we restricted ourselves to analysing two selected models picked out from both sequences at $T_{\text{eff}} \approx 10\,000\text{K}$. Hereafter, we shall denote these template models as OCWD (oxygen-core WD) and HECWD (helium-core WD) models. We begin by examining the shape of the Ledoux term and the Brunt-Väisälä frequency in Figs 9 and 10 (middle and bottom panels, respectively). To make easier the association amongst the various chemical transitions and the corresponding features in N , we have also included the internal chemical profiles in these figures (upper panels).

For the case of the OCWD model, the most outstanding characteristic in the shape of N is the peaked feature at $\log(1 - M_r/M_*) \approx -0.2$ (Fig. 9). This is directly associated with the abrupt variation in the oxygen abundance at such very deep layers. On the other hand, the oxygen/helium interface is responsible for the less narrow neighbouring peak in N ; finally, at $\log(1 - M_r/M_*) \approx -3.25$, there is a broad, smooth bump which is caused by the helium/hydrogen transition region. The shape of N corresponding to the HECWD model is documented in the bottom panel of Fig. 10. As can be appreciated

from the figure, in this case the only local feature present in N is that resulting from the helium/hydrogen chemical transition zone. The comparison of the Brunt-Väisälä frequency for both models deserves some comments. As is well known, any local feature in the Brunt-Väisälä frequency constitutes a source for trapping or confinement of modes (see Brassard et al. 1992; Córscico et al. 2002). As a result, we expect the mode-trapping/confinement properties of OCWD model to be considerably more featured than those of the HECWD model. The other point worthy of comment is the fact that N in the HECWD model shows slightly greater values at the innermost core region than for the OCWD case. Although this seems to be a subtle difference, it causes the periods to be shorter and the asymptotic period spacing to be somewhat smaller in the case of the OCWD model.

In what follows, we comment on the results we obtained for the pulsational properties of our models. Specifically, we have computed the adiabatic, non-radial g -modes of low degree ($\ell = 1, 2, 3$) with overtones covering a wide period window of 50–2000 s. In addition, related quantities such as oscillation kinetic energy (E_{kin}) and first-order rotational splitting coefficient ($C_{\ell,k}$) have been obtained for each computed mode. We mention that the radial eigenfunction

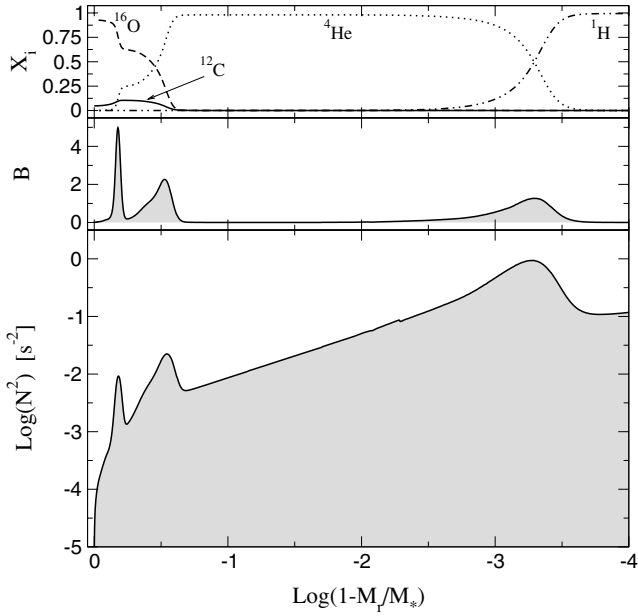


Figure 9. The internal chemical profile, the Ledoux term and the Brunt-Väisälä frequency (upper, middle and bottom panel, respectively) in terms of the outer mass fraction, corresponding to a selected $0.33 - M_\odot$ oxygen-core WD model at $T_{\text{eff}} \approx 10000\text{K}$. Note that N exhibits a peaked feature at the innermost region of the model. It is a direct consequence of the steep change of the ^{16}O abundance at $\text{log}(1 - M_r/M_*) \approx -0.2$. The remainder, less narrow features, are associated with the oxygen/helium and the helium/hydrogen interfaces.

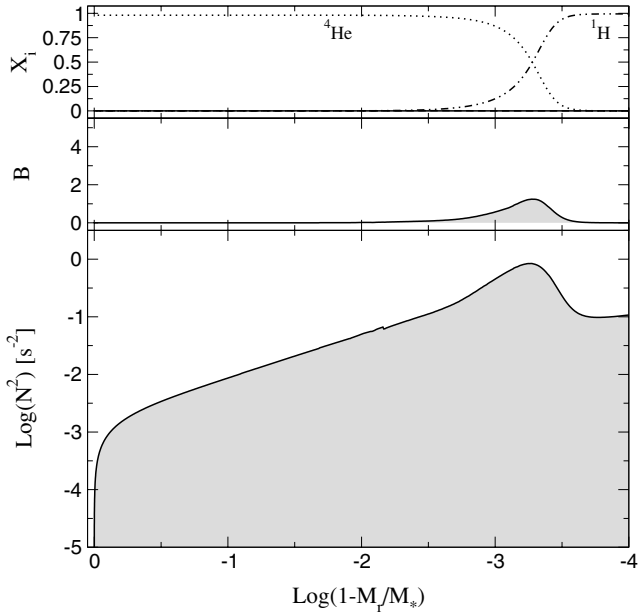


Figure 10. The same as Fig. 9, but for a helium-core WD model of $0.33 - M_\odot$ at the same effective temperature. In this case, the only feature characterizing the shape of the Brunt-Väisälä frequency is that associated with the helium/hydrogen interface (the only chemical transition region in this model).

$(\delta r/r)$ is normalized to 1 at the surface. The main observable quantities in pulsating WD stars are the periods (P_k) and the forward period spacing ($\Delta P_k = P_{k+1} - P_k$). Thus, we shall employ these quantities as the main discriminants to demonstrate the different pulsational behaviours associated with OCWD and HECWD model stars.

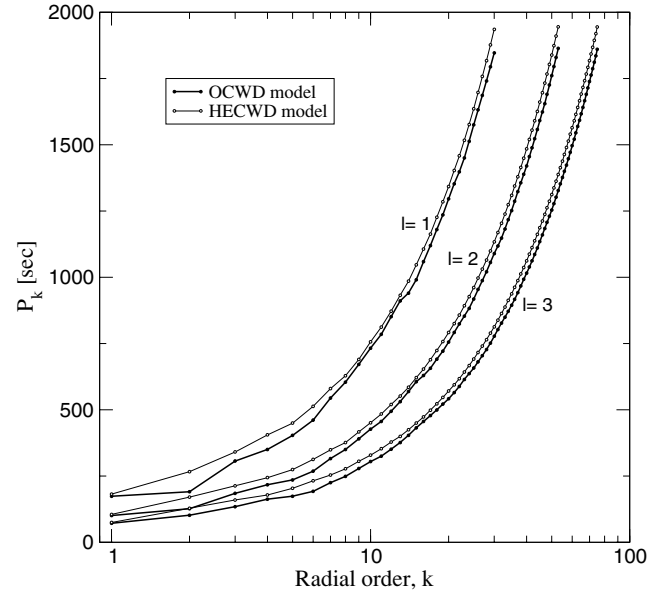


Figure 11. Periods as a function of the overtone number for $\ell = 1, 2$ and 3 corresponding to OCWD (thick lines, filled dots) and HECWD (thin lines, empty dots) models.

We begin by examining Fig. 11, which shows the periods as a function of the overtone number for $\ell = 1, 2$ and 3 corresponding to OCWD (thick lines) and HECWD (thin lines) models. Note that *all* the periods corresponding to HECWD model are longer than for the case of the OCWD one. As mentioned, this is a consequence of N being slightly larger at the innermost core region in the case of the HECWD model. Note also for this model the near uniformity in the period distribution as compared with the OCWD case (see below).

In Fig. 12, we show ΔP_k , $\log(E_{\text{kin}})$ and $C_{\ell,k}$ (upper, middle and bottom panels, respectively) in terms of periods, for $\ell = 1, 2, 3$ (left, centre and right) corresponding to the OCWD model. Fig. 13 depicts the same quantities, but for the case of the HECWD model. We begin by examining the ΔP_k distribution in Fig. 12. As expected, the spacing of consecutive periods is markedly featured, reflecting the three sources of trapping/confinement of modes corresponding to each of the three chemical interfaces. An inspection of the figures reveals that the amplitude of ΔP_k corresponding to the OCWD model is typically larger as compared with the HECWD model. Note also the strong minima in ΔP_k in the OCWD model. These minima correspond to modes *partially confined* to the deepest regions of the star. Indeed, at the high-density zone bounded by the stellar centre and by $\text{log}(1 - M_r/M_*) \approx -0.2$, such modes have larger amplitudes of their eigenfunctions as compared with those of the neighbouring overtones. Consequently, such modes must exhibit local maxima in the E_{kin} distribution (see middle panels of Fig. 12). In contrast, the much less pronounced minima exhibited by ΔP_k in the HECWD model are related to trapped modes in the outer layers. Thus, these modes are characterized by low kinetic energy values (Fig. 13). Finally, we note that the distribution of the $C_{\ell,k}$ values corresponding to the HECWD model exhibits less structure as compared with the case of the OCWD one, particularly regarding to the short- and intermediate-period domains.

Clearly, from the above considerations, we conclude that there exist marked differences between the adiabatic pulsational properties of helium- and oxygen-core low-mass WDs. This, in principle,

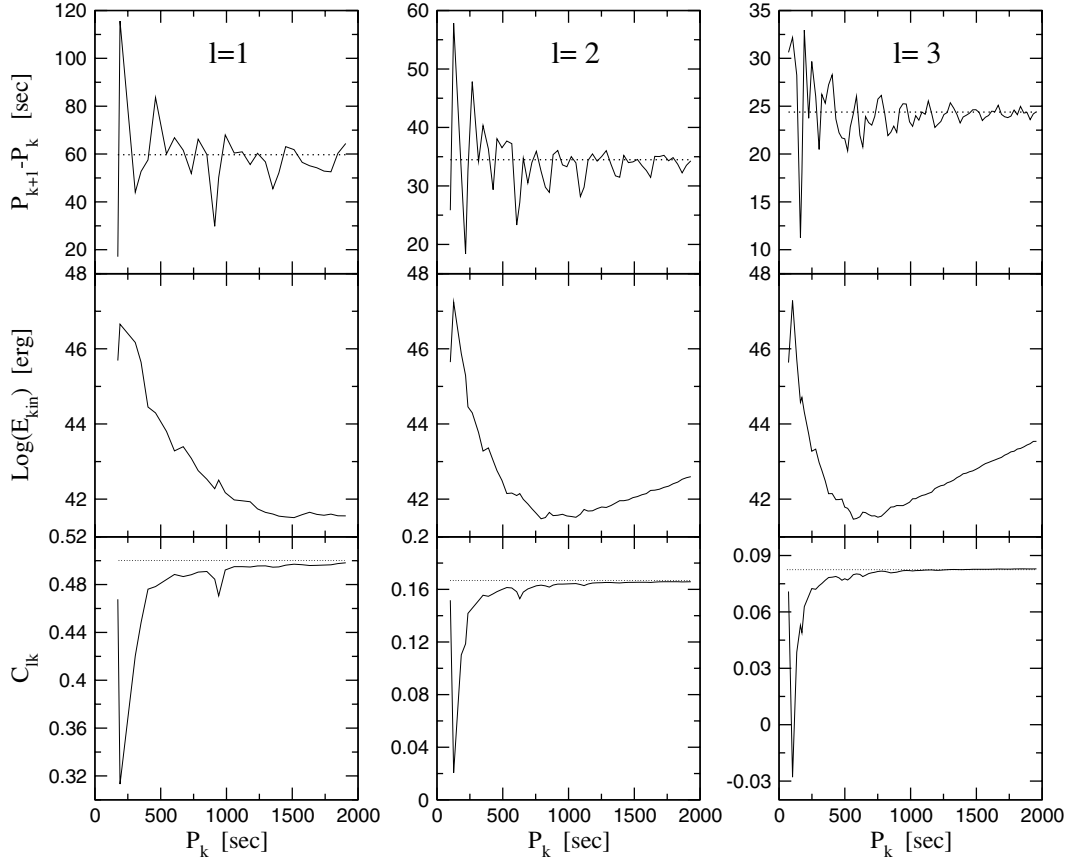


Figure 12. The forward period spacing (upper panels), the logarithm of the kinetic energy (middle panels) and the first order rotational splitting coefficients (lower panels), in terms of the periods for g -modes with $\ell = 1$ (left-hand panels), $\ell = 2$ (centre panels) and $\ell = 3$ (right-hand panels), for the same WD model analysed in Fig. 9 (OCWD models). In the interest of clarity, we have omitted the symbols representing pulsation modes. Dotted lines represent the asymptotic period spacing (upper panels) and the asymptotic value of $C_{\ell,k}$ (lower panels).

turns the asteroseismological techniques usually employed in variable WD studies into an important tool for distinguishing both types of stars.

4.2 Non-adiabatic pulsations

Finally, we comment on the main results from non-adiabatic pulsation calculations of the oxygen-core WD models. We emphasize that for the WD regime, we modelled convection according to the mixing-length theory, setting the mixing length to 1.5 pressure scale-heights. The grey domain in Fig. 14 shows the extension of the superficial convection zone as a function of effective temperature. Note that at $T_{\text{eff}} \approx 10\,000\text{K}$, below which modes are found to be unstable (see below), the base of the convection zone sinks appreciably into the star. The linear non-adiabatic oscillation spectra were computed for dipolar ($\ell = 1$) g -modes in the period range between 100 and about 1200 s using the same Riccati shooting method as referred to in Gautschy, Ludwig & Freytag (1996) (see also Gautschy & Althaus 2002). The non-adiabatic computations were done assuming a frozen-in convective flux.

Fig. 15 displays the modal diagram for the $0.33 - M_{\odot}$ oxygen-core WD sequence. Specifically, the figure depicts the periods of the lowest order $\ell = 1$ modes as a function of effective temperature. Overstable modes are indicated by black dots. Like radial orders are connected by a continuous line. The highest order shown is $k = 18$. An instability domain is found that starts at $\log T_{\text{eff}} = 3.993$

and continues below the cool end of the model series analysed. Only modes with periods exceeding about 680 s become unstable. A striking feature concerns the position of the blue edge: it does not depend on the radial order, i.e. on the length of the periods. Furthermore, a survey computation showed that the saturation of the excitation must be beyond $k = 30$. In other words, we did not find the long-period edge of the instability domain.

Fig. 16 shows the imaginary parts of the eigenvalues as a function of T_{eff} . Note that the maximum of the instability, i.e. the minimum of σ_1 , is encountered very close to the blue edge. The excitation rates decline quickly towards lower temperatures. Notice, as referred to in the last paragraph, that the instability (i.e. the magnitude of σ_1) continues to get stronger to higher overtone numbers.

We mention that the non-adiabatic computations included the effect of nuclear burning, i.e. the ϵ -mechanism. However, we considered only the equilibrium situation, neglecting the perturbation of the abundance of the reactants. We find that the work integrals have no appreciable contribution from the ϵ -mechanism. A point of interest is the question if pulsations might trigger a very late hydrogen shell flash. Based on the fact that the eigenfunctions have very low amplitudes in hydrogen-burning regions, we do not expect a pulsation-induced thermonuclear flash to be feasible.³

³ The g -mode pulsations' preponderant horizontal displacements are unlikely to disturb the geometry of the nondegenerate H-burning shell such as to trigger a thermal runaway.

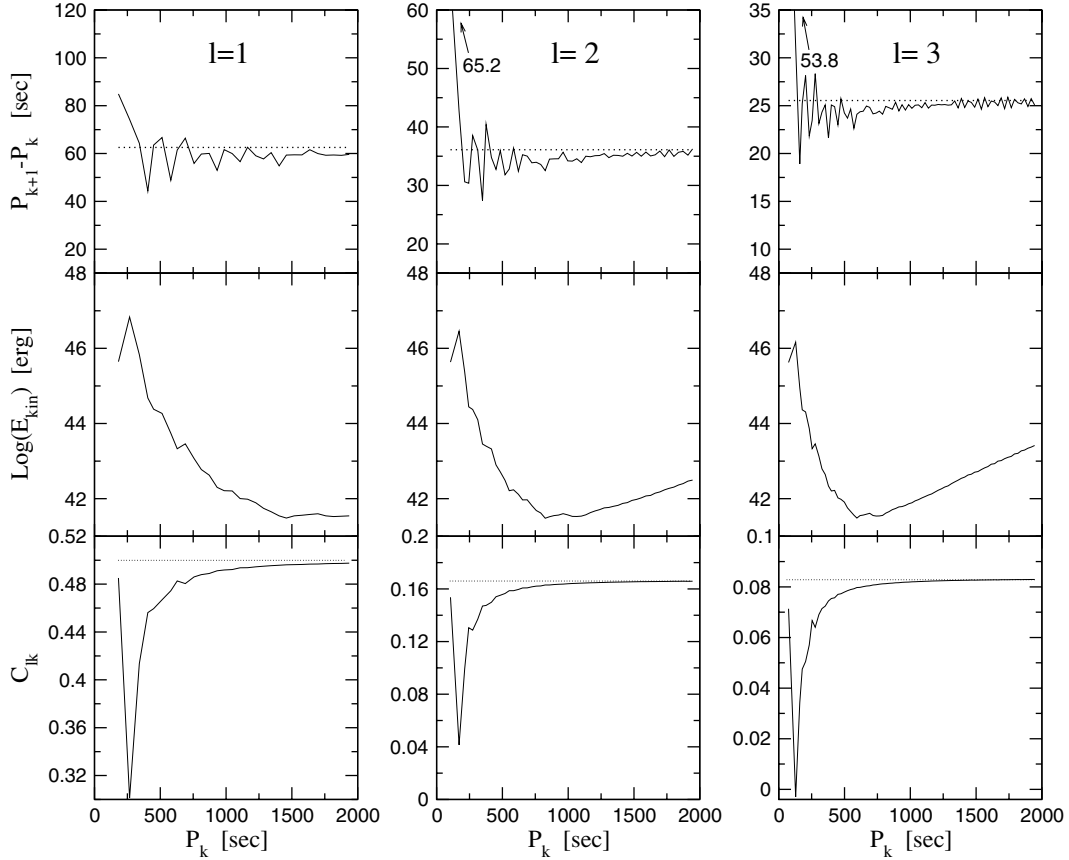


Figure 13. The same as Fig. 12, but for the model analysed in Fig. 10 (HECWD model).

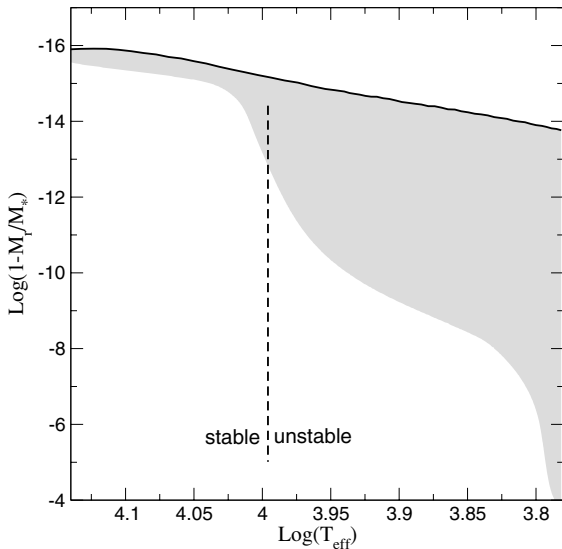


Figure 14. Location of the convection zone as given by the outer mass fraction as a function of effective temperature (grey domain). The vertical, dashed line indicates the value of effective temperature below which g -modes become unstable. The thick line marks the outer edge of the convection zone which is near the location of the photosphere.

Finally, since no convection–pulsation interaction was considered, the non-adiabatic results indicate at the very best that the κ mechanism destabilizes low-degree modes of intermediate order. The action of convection can still modify the picture considerably, even on a qualitative level.

5 CONCLUSIONS

Motivated by theoretical evidence suggesting that some of the presumed low-mass, helium-core WDs could actually be WDs with oxygen cores (Iben & Tutukov 1985; Han et al. 2000), we explored in this paper the evolution of low-mass WDs with oxygen cores in a self-consistent way with the predictions of nuclear burning, the chemical evolution caused by time-dependent element diffusion and the history of the WD progenitor. We concentrated on an oxygen-core WD remnant of mass $0.33 M_{\odot}$. The evolutionary stages prior to the WD formation were also fully accounted for by computing the conservative binary evolution of an initially $2.5 - M_{\odot}$ Population I star with a $1.25 M_{\odot}$ companion, and with an orbital period of $P_i = 3d$. In addition, we explored the adiabatic and non-adiabatic pulsational properties of the resulting WD models.

As for the main evolutionary results, we mention the following.

(i) The evolution of the star is characterized by the occurrence of several episodes of thermonuclear flashes due to unstable hydrogen burning at the base of the hydrogen-rich envelope.

(ii) Diffusion processes play an important role in the evolution of low-mass oxygen-core WDs. In particular, the remaining amount of hydrogen, shortly after hydrogen flashes have ceased, is markedly lower when diffusion is considered. This fact produces a different cooling history even at very late stages of the evolution. In particular, element diffusion prevents hydrogen burning from being the main energy source for most of the evolution of a low-mass, oxygen-core WD. As a result, cooling ages are roughly a factor of 2–3 smaller than ages derived from models neglecting diffusion.

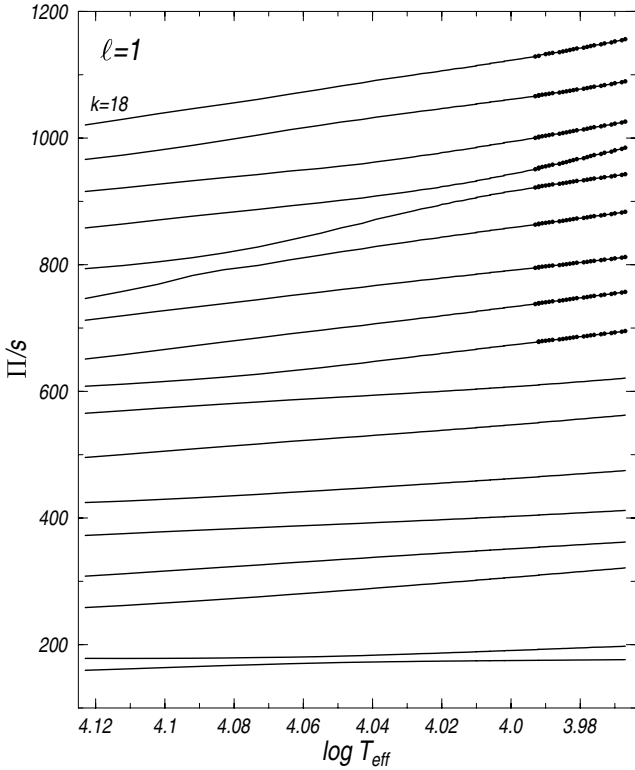


Figure 15. Modal diagram for $\ell = 1$ of the $0.33 - M_{\odot}$ oxygen-core WD sequence. The dots on some intermediate-order modes indicate their instability.

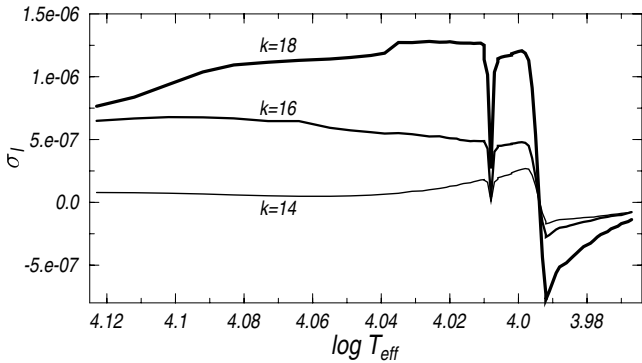


Figure 16. The same as Fig. 15, but for the imaginary part of selected eigenfrequencies. Negative numbers mean oscillatory instability. The radial order of the eigenmodes is labelled on the graph.

(iii) As compared with the helium-core counterparts, low-mass, oxygen-core WDs cool much faster once they have settled on their final cooling track. In particular, at advanced stages, to reach a given temperature, the oxygen-core WD evolves about twice as fast as a helium-core WD.

The main pulsational properties of our models are as follows.

(i) The structure of the pulsational spectrum of the oxygen-core WD models is notably richer than that of the helium-core ones. This fact is apparent from the period spacing diagrams, which exhibit large amplitudes of trapping/confinement imprints.

(ii) The presence of an oxygen core is responsible for some *partially confined* modes that are characterized by comparatively large

values of kinetic energy and strong minima in a period-spacing diagram.

(iii) Modes with periods longer than about 680 s become unstable at effective temperatures below about 10 000 K.

We conclude that both the pulsational and evolutionary properties of low-mass, carbon/oxygen WDs turn out to be substantially different from those of the helium-core WDs. In particular, our results suggest that a discrimination between helium-core and carbon/oxygen-core WDs by means of asteroseismology is possible if low-mass WDs were in fact found to pulsate as ZZ Ceti-type variables. Despite the lack of signs of variability in low-mass WDs so far, we consider the monitoring of low-mass WDs to find variable candidates to be worthwhile.

Complete tabulations of the results of the present paper are available at <http://www.fcaglp.unlp.edu.ar/evolgroup/>.

ACKNOWLEDGMENTS

We warmly acknowledge our referee Michael Montgomery for his suggestions and comments, which improved the original version of this work. We also thank the financial support by the Instituto de Astrofísica de La Plata. This research has made use of NASA's Astrophysical Data System Abstract Service.

REFERENCES

- Alexander D. R., Ferguson J. W., 1994, *ApJ*, 437, 879
 Althaus L. G., 1996, PhD thesis, Univ. La Plata
 Althaus L. G., Serenelli A. M., Benvenuto O. G., 2001a, *MNRAS*, 323, 471
 Althaus L. G., Serenelli A. M., Benvenuto O. G., 2001b, *MNRAS*, 324, 617
 Althaus L. G., Serenelli A. M., Córscico A. H., Montgomery M. H., 2003, *A&A*, 404, 593
 Bradley P. A., 1998, *Baltic Astron.*, 7, 111
 Brassard P., Fontaine G., Wesemael F., Kawaler S. D., Tassoul M., 1991, *ApJ*, 367, 601
 Brassard P., Fontaine G., Wesemael F., Hansen C. J., 1992, *ApJS*, 80, 369
 Burgers J. M., 1969, *Flow Equations for Composite Gases*. Academic Press, New York
 Castellani V., Chieffi A., Pulone L., Tornambe A., 1985, *ApJ*, 296, 204
 Caughlan G. R., Fowler W. A., Harris M. J., Zimmerman B. A., 1985, *Atomic Data and Nuclear Data Tables*, 35, 198
 Caughlan G. R., Fowler W. A., 1988, *Atomic Data and Nuclear Data Tables*, 40, 284
 Córscico A. H., 2003, PhD thesis, Univ. La Plata
 Córscico A. H., Althaus L. G., Benvenuto O. G., Serenelli A. M., 2001, *A&A*, 380, L17
 Córscico A. H., Althaus L. G., Benvenuto O. G., Serenelli A. M., 2002, *A&A*, 387, 531
 Driebe T., Schönberner D., Blöcker T., Herwig F., 1998, *A&A*, 339, 123
 Edmonds P. D., Grindlay J. E., Cool A. M., Cohn H. N., Lugger P. M., Bailyn C. D., 1999, *ApJ*, 516, 250
 Edmonds P. D., Gilliland R. L., Heinke C. O., Grindlay J. E., Camilo F., 2001, *ApJ*, 557, L57
 Gautschy A., Althaus L. G., 2002, *A&A*, 382, 141
 Gautschy A., Ludwig H.-G., Freytag B., 1996, *A&A*, 311, 493
 Han Z., 1998, *MNRAS*, 296, 1019
 Han Z., Tout C. A., Eggleton P. P., 2000, 319, 215
 Han Z., Podsiadlowski Ph., Maxted P. F. L., Marsh T. R., Ivanova N., 2002, *MNRAS*, 336, 449
 Hansen B. M. S., Phinney E. S., 1998, *MNRAS*, 294, 557
 Iben I., Jr, Livio M., 1993, *PASP*, 105, 1373
 Iben I., Jr, MacDonald J., 1986, *ApJ*, 301, 164

- Iben I., Jr, Tutukov A. V., 1985, *ApJS*, 58, 661
- Iben I., Jr, Webbink R. F., 1989, in Wegner G., ed., *IAU colloq.* 114, White dwarfs. Springer-Verlag, Berlin, p. 477
- Iglesias C. A., Rogers F. J., 1996, *ApJ*, 464, 943
- Landsman W., Aparicio J., Bergeron P., Di Stefano R., Stecher T. P., 1997, *ApJ*, 481, L93
- Lundgren S. C., Cordes J. M., Foster R. S., Wolszczan A., Camilo F., 1996, *ApJ*, 458, L33
- Magni G., Mazzitelli I., 1979, *A&A*, 72, 134
- Marsh T. R., 1995, *MNRAS*, 275, L1
- Marsh T. R., Dhillon V. S., Duck S. R., 1995, *MNRAS*, 275, 828
- Maxted P. F. L., Marsh T. R., Moran C. H. J., Zan Z., 2000, *MNRAS*, 314, 334
- Metcalfe T. S., 2003, *ApJ*, 587, L43
- Moran C., Marsh T. R., Bragaglia A., 1997, *MNRAS*, 288, 538
- Orosz J. A., Wade R. A., Harlow J. J. B., Thorstensen J. R., Taylor C. J., Eracleous M., 1999, *AJ*, 117, 1598
- Paczyński B., 1976, in Eggleton P. P., Mitton S., Whelan J., eds, *Structure and Evolution of Close Binaries*. Kluwer, Dordrecht, p. 55
- Rogers F. C., Iglesias C. A., 1992, *ApJS*, 79, 507
- Sarna M. J., Ergma E., Antipova J., 2000, *MNRAS*, 316, 84
- Serenelli A. M., 2002, PhD, Univ. La Plata
- Serenelli A. M., Althaus L. G., Rohrmann R. D., Benvenuto O. G., 2002, *MNRAS*, 337, 1091
- Taylor J. M., Grindlay J. E., Edmonds P. D., Cool A. M., 2001, *ApJ*, 553, L169
- van Kerkwijk M. H., Bell J. F., Kaspi V. M., Kulkarni S. R., 2000, *ApJ*, 530, L37
- Wallace R. K., Woosley S. E., Weaver T. A., 1982, *ApJ*, 258, 696

This paper has been typeset from a \TeX/L\AA\TeX file prepared by the author.